ORGANOMETALLICS

pubs.acs.org/Organometallics Article

# Modular Design Strategy toward Second-Generation Tridentate Carbodiphosphorane N,C,N Ligands with a Central Four-Electron Carbon Donor Motif and Their Complexes

Marius Klein and Jörg Sundermeyer*

Cite This: *Organometallics* 2021, 40, 2090–2099 Read Online

ACCESS | Metrics & More | Article Recommendations | Supporting Information

**ABSTRACT:** The reaction of *sym*-bis(*P*-chlorodiphenyl)-carbodiphosphorane (**1**) with difunctional nucleophiles leads to carbodiphosphoranes carrying two additional chelating N-donor functionalities. A proof of concept is demonstrated by the synthesis and characterization of *sym*-bis(3,5-dimethyl-1*H*-pyrazol-1-yl)-carbodiphosphorane ($CDP(^{3,5\text{-}Me}Pz)_2$, **2**) and *sym*-bis(pyridin-2-yloxy)carbodiphosphorane ($CDP(O\text{-}^2Py)_2$, **3**). Due to their superbasic central two-/four-electron carbon donor functionality, these neutral ligands are electronically flexible to act as neutral six- or eight-electron donors, as pincer ligand templates, or as two geminally metal bridging ligands. Their potential to form mono- and dinuclear complexes involving two 6-ring or two 5-ring N,C-chelate ring motives has been explored. Complexes of **2** and **3** with *fac*-$[M(CO)_3]$ fragments (ls $d^6$; M = Cr, Mo, W) were used as spectroscopic probes. They reveal a strong $\sigma$-donor and potential $\pi$-donor ability of the central carbon donor pushing electron density for enhanced M−CO back-bonding into the metal d orbitals. DFT calculations consolidate this observation. Dinuclear and multinuclear $d^{10}$ Cu(I) complexes have been formed and structurally investigated upon treating these CDP ligands **2** and **3** with CuX (X = Cl, Br, I).

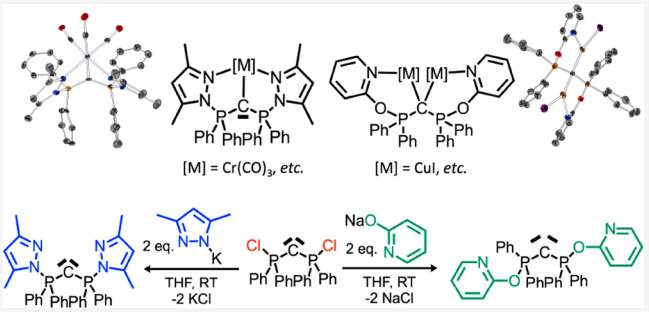


## INTRODUCTION

Hexaphenylcarbodiphosphorane was first synthesized in 1961.[1] For many years, organometallic chemistry mainly focused on this particular monofunctional carbodiphosphorane (CDP), a neutral zwitterionic carbon donor with a donor capability of potentially four electrons.[2−5] Traditionally, the bonding in CDPs has been discussed in terms of zwitterionic, double ylidic, or donor−acceptor resonance forms with some preference for the ylidic form. The other resonance form suggesting a CDP bonding situation best described as a donor−acceptor complex of two phosphines stabilizing a formally zerovalent carbon atom of coordination number 2 has been much promoted by Frenking and co-workers.[6−10] On the basis of their DFT analyses the central carbon atom can act as an acceptor atom in its excited singlet ($^1D$) state stabilized by the $\sigma$-donating phosphine ligands. The two lone pairs characteristic for such a carbon(0) complex or "carbone" are differentiated into one of $\pi$ symmetry, partially stabilized by back-bonding into the two phosphine LUMOs of $\pi$ symmetry, while the other carbon lone pair of $\sigma$ symmetry is the CDP orbital typically addressed first for $\sigma$ bonds toward metal cations (or protons).[11] Without a doubt, the Frenking carbone model is an inspiration, especially if related phosphine (or L) complexes of higher homologues of elemental carbon and other elements are envisaged or analyzed by DFT calculations.

Some time ago, the very strong four-electron $\sigma$- + $\pi$-donor character of this neutral CDP carbon ligand was proven experimentally in organometallic complexes of highly $\pi$ acidic $d^0$-$[ReO_3]^+$ fragments.[12] In contrast, Lewis acids without a LUMO of $\pi$ symmetry (similar to protons) address both the HOMO and HOMO-1 of the CDP, preferentially forming dinuclear complexes with two dative $\sigma$ bonds of the bridging four-electron-donor carbon atom. These versatile properties make CDPs attractive as ligands in coordination chemistry.[2−4] Common synthetic strategies for the synthesis of CDPs involve deprotonation,[1,13] dehydrohalogenation,[14] or dehalogenation[11,15,16] of the corresponding precursors such as $[HC(PR_3)_2]X$, $[H_2C(PR_3)_2]X_2$, or $[ClC(PR_3)_2]X$. CDPs have also been used as central building blocks in pincer ligands, thus extending their potential as templates in organometallic chemistry. Rhodium and platinum precursor complexes do react with hexaphenylcarbodiphosphorane to yield cyclometalated, formally dianionic C,C,C pincer complexes.[17−21]

Received: April 10, 2021
Published: June 28, 2021

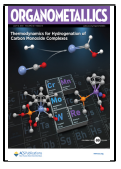

Downloaded via HIMACHAL PRADESH UNIV on August 11, 2021 at 16:01:19 (UTC).
See https://pubs.acs.org/sharingguidelines for options on how to legitimately share published articles.

ACS Publications

© 2021 The Authors. Published by American Chemical Society



https://doi.org/10.1021/acs.organomet.1c00231
*Organometallics* 2021, 40, 2090−2099

Isolation of bis-ortho-lithiated $Li_2CDP$[22] allows transferring this dianionic C,C,C pincer ligand to s-, p-, d-, and f-metal centers.[23] P,C,P pincer CDP complexes have been introduced by Peringer[24−28] and further investigated by Langer.[29−31] For a long time, they had only been characterized in the form of their complexes. Only recently, the free ligand base has $C(dppm)_2$ been isolated, characterized, and used in ligand transfer reactions.[32] In the field of N,C,N carbodiphosphorane pincer ligands, the Zhu and Sundermeyer groups reported the synthesis of CDP complexes incorporating two phosphorus-bound 2-pyridyl donor functionalities.[33,34] The free pincer ligand was obtained following the Appel strategy,[16] a radical reaction of 2-Py-$PPh_2$ and $CCl_4$.[33] Notably, several years before, a mono-2-pyridyl-substituted carbodiphosphorane was synthesized by Alcarazo et al. in order to investigate heterobimetallic complexes; however, tridentate or pincer-type CDP ligands were not considered or realized.[35] Recently, the Gessner group has reported the coordination capability of an bis-*P*-piperidino-substituted CDP ligand.[36a] They stated that the N-donor character toward $d^{10}$-$Zn^{2+}$ is either nonexistent or rather weak. Both the electron-withdrawing character of the phosphonio group attached to the proposed N-donor atom and an unfavorable bite defined by potentially two annelated four-membered chelate rings hinder this ligand from being a privileged tridentate donor. In order to design new pincer type N,C,N ligands via a construction kit and a different strategy from that which we previously reported, we decided to study the reaction of ambident N,N- and N,XO-anion building blocks with the known *sym*-bis(*P*-chlorodiphenyl)carbodiphosphorane ($CDP-Cl_2$) as a P-electrophile.[37]

## RESULTS AND DISCUSSION

$CDP-Cl_2$ (**1**) can be converted to *sym*-bis(3,5-dimethyl-1*H*-pyrazol-1-yl)carbodiphosphorane ($CDP(^{3,5\text{-}Me}Pz)_2$, **2**) and *sym*-bis(pyridin-2-yloxy)carbodiphosphorane ($CDP(O\text{-}^2Py)_2$, **3**) by reaction with 2 equiv of potassium 3,5-dimethyl-1*H*-pyrazolate and sodium-2-pyridinolate, respectively. After 18 h at room temperature in THF the conversions were complete, as monitored by $^{31}P\{^1H\}$ NMR. Light green $CDP(^{3,5\text{-}Me}Pz)_2$ (**2**) was isolated in 77% yield and gray $CDP(O\text{-}^2Py)_2$ (**3**) in close to quantitative yield in their free ligand base forms (Scheme 1). In sharp contrast to the previously described *sym*-bis(2-pyridyl)tetraphenylcarbodiphosphorane $CDP(^2Py)_2$, the new N-functional CDPs **2** and **3** both do not show any photoluminescence[33] or triboluminescence.[38] As expected, $^{31}P\{^1H\}$ NMR spectra display singlets for **2** (8.9 ppm, $C_6D_6$) and for **3** (23.1 ppm, $CD_2Cl_2$), a trend deviating from the parent hexaphenylcarbodiphosphorane (4.3 ppm, $C_6H_5Cl$)[39] or $CDP(^2Py)_2$ (−5.6 ppm, $C_6D_6$).[33] However, our observation is in accord with the relatively high group electronegativity of the introduced N- and O-anions substituting electronegative P-chloro or P-fluoro substituents in *sym*-$CDP-Cl_2$ (**1**) (22.7 ppm, $C_6D_6$) and *sym*-$CDP-F_2$ (43.2 ppm, $C_6D_6$).[40]

**Scheme 1. Synthesis of the Novel Tridentate N,C,N Carbodiphosphorane Ligands 2 and 3**

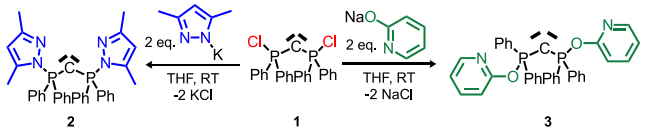


Since no crystal structure of the free ligands **2** and **3** could be obtained so far by applying various crystallization techniques, DFT calculations at the PBE-D3(BJ)/def2-TZVPP level of theory were performed in order to gain a deeper insight into the gas-phase structures of **2** and **3** (see Figures S-87−S-94). A quantum mechanical analysis reveals that both structures show the arrangement of two coplanar phenyl rings attached to different phosphonio groups. The other two phenyl rings point with their *ortho* hydrogen atoms toward the electron-rich central carbon atom with its formally two electron lone pairs. This phenomenon of stabilization by $\pi$-stacking and weak intramolecular $C\cdots H_{ortho}$ interactions has also been observed[33,41] and discussed[33,42] for other CPDs. The repulsive nature of the substituents and carbon lone pairs forces the 3,5-dimethyl-1*H*-pyrazol-1-yl groups of **2** and the pyridin-2-yloxy groups of **3** into an *anti* conformation. Not surprisingly, DFT calculations propose that the HOMO-1 can be interpreted as a lone pair orbital of $\sigma$ symmetry and the HOMO as one of $\pi$ symmetry in both **2** and **3** (Figure 1). This is supported by a natural bond orbital (NBO) analysis, where the atomic partial charge of the central carbon $q(C)$ was calculated at the PBE-D3(BJ)/def2-TZVPP level of theory. For **2** $q(C)$ is −1.41 e and for **3** $q(C)$ is −1.38 e.

In accord with previously reported proton affinities (PA) of carbodiphosphoranes,[10,33] DFT calculations on **2** give PA values of 282.6 and 186.5 kcal/mol for the first and second protonations, whereas the corresponding values are 287.6 and 192.3 kcal/mol for **3**. Upon the first and second protonations of the neutral CDPs the negative charge $q(C)$ becomes less negative: the $q(C)$ value of $[\mathbf{2H}]^+$ is −1.33 e, that of $[\mathbf{2H_2}]^{2+}$ is −1.17 e, that of $[\mathbf{3H}]^+$ is −1.36 e, and that of $[\mathbf{3H_2}]^{2+}$ is −1.19 e. The DFT results clearly show that considerable electron density is located at the imidazole and pyridine N-donor atoms at a bite angle perfectly suitable for a double-chelating bonding situation. Therefore, we anticipated that, in contrast to Gessner's bis(amino)-CDP[36a] and our tetra- and hexaamino-CDPs,[34b] we might have generated new tridentate or even pincer-type CDP ligands.

In order to evaluate the coordinative potential of these tri- or tetradentate six- or eight-electron-donor ligands, **2** and **3** were reacted with $[M(CO)_3(NCMe)_3]$ (M = Cr, Mo, W) in THF. The products *fac*-$[M(CO)_3(CDP(^{3,5\text{-}Me}Pz)_2)]$ (**4a**, **5**, and **6**)

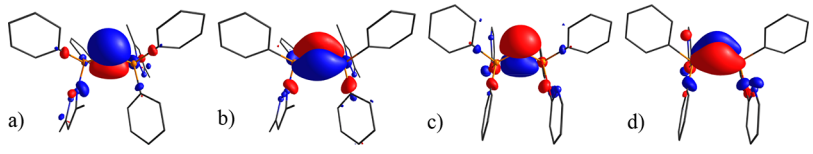


**Figure 1.** Kohn−Sham orbitals of the HOMO-1 (a) and HOMO (b) of **2** and the HOMO-1 (c) and HOMO (d) of carbodiphosphorane **3** calculated for the optimized $S_0$ state geometry (isovalue 0.05). Calculations were performed at the PBE-D3(BJ)/def2-TZVPP level of theory.


https://doi.org/10.1021/acs.organomet.1c00231
Organometallics 2021, 40, 2090−2099

**Scheme 2. Synthesis of Novel Carbodiphosphorane Carbonyl Complexes of *sym*-Bis(3,5-dimethyl-1*H*-pyrazol-1-yl)carbodiphosphorane (2) and *sym*-Bis(pyridin-2-yloxy)carbodiphosphorane (3)**

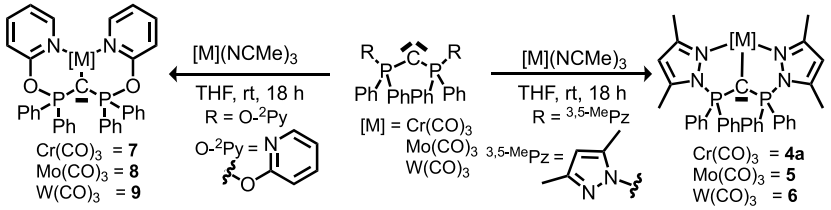


and *fac*-[M(CO)$_3$(CDP(O-$^2$Py)$_2$)] (**7**–**9**) were isolated in good yields of between 54% and 85% (Scheme 2).

The Cr and Mo complexes **4a**, **5** and **7**, **8** were crystallized via layering a solution in dichloromethane or chloroform with *n*-pentane. The results of single-crystal XRD analyses are displayed in Figure 2.

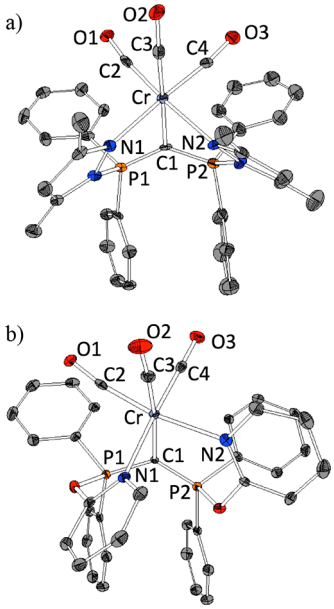


**Figure 2.** XRD molecular structures of (a) *fac*-[Cr(CO)$_3$(CDP($^{3,5\text{-Me}}$Pz)$_2$)] (**4a**) and (b) *fac*-[Cr(CO)$_3$(CDP(O-$^2$Py)$_2$)] (**7**). The isostructural *fac*-[Mo(CO)$_3$(CDP($^{3,5\text{-Me}}$Pz)$_2$)] (**5**) and *fac*-[Mo(CO)$_3$(CDP(O-$^2$Py)$_2$)] (**8**) are displayed in Figure S-80 of the Supporting Information. Hydrogen atoms and solvent molecules have been omitted for clarity; thermal ellipsoids are set at 50% probability. For details see the Supporting Information.

All isostructural complexes crystallize in the triclinic space group $P\bar{1}$ with two units in their unit cells. As has already been observed for related CDP($^2$Py)$_2$ ligand complexes,[33] the central atoms are coordinated in a slightly distorted facial configuration. This is due to a strong thermodynamic *trans* effect of the $\pi$-acidic carbonyl ligands directing the much less $\pi$-acidic pincer donor atoms into a facial array. Both 3,5-dimethyl-1*H*-pyrazol-1-yl donor functionalities are part of five-membered chelate rings and both pyridin-2-yloxy units are part of six-membered chelate rings with respect to the central carbon donor. Selected bond distances and angles for **4a**, **5**, **7**, and **8** are displayed in Table 1. As expected, the M–C1, M–N and M–CO distances increase when the 3d metal Cr in **4a** and **7** is replaced by the 4d metal Mo in **5** and **8**. For example, the prominent M–C1 distance increases from 2.220(3) Å (**4a**, Cr) to 2.339(4) Å (**5**, Mo) and from 2.264(2) Å (**7**, Cr) to 2.3713(17) Å (**8**, Mo). This is consistent with the presence of M–C single bonds, without any $\pi$-dative contribution, as expected for such 18-valence-electron metal centers without matching metal-centered LUMOs and with respect to the differences in covalent radii of Cr (1.39 Å) and Mo (1.54 Å).[43] While the P1–C1–P2 angle increases in the more rigid 5-ring chelate structures of **2** rising 134.8(2)° (**4a**, Cr) to 136.2(3)° (**5**, Mo), a less pronounced increase is registered in the more flexible 6-ring chelate structures of **3** from 129.01(13)° (**7**, Cr) to 129.91(11)° (**8**, Mo). For the same metal, the less constrained annelated 6-ring chelates display shorter M–C1 bonds and the more constrained 5-ring chelates longer M–C1 bonds. The trend to shorter M–C1 bonds correlates with a tendency for slightly longer M–N bonds to both pyridyl sp$^2$ donor atoms in **7** and **8** in comparison to pyrazolyl sp$^2$ donor atoms in **4a** and **5**. Due to the additional methyl groups at the 3,5-dimethyl-1*H*-pyrazol-1-yl units and a much more constrained situation in tridentate chelate complexes of **2**, the coplanar $\pi$-stacked phenyl rings previously observed in the free ligand base deviate from coplanarity and experience less $\pi$ stacking (Figure 2a). However, less constrained pyridin-2-yloxy complexes **7** and **8** with their smaller P1–C1–P2 angles display such pairs of nearly coplanar phenyl rings in the crystalline solid state: interplanar angles of both phenyl rings are as follows: **4a**, 22.15°; **5**, 24.52°; **7**, 9.65°; **8**, 9.89° (Figure 2b). For details see Figures S-83–S-86 in the Supporting Information.

**Table 1. Selected Bond Distances (Å) and Angles (deg) for 4a, 5, 7, and 8**

| | 4a | 5 | 7 | 8 |
|---|---|---|---|---|
| M–C1 | 2.220(3) | 2.339(4) | 2.264(2) | 2.371(2) |
| M–N1 | 2.175(4) | 2.318(5) | 2.190(2) | 2.320(2) |
| M–N2 | 2.173(4) | 2.300(4) | 2.2408(18) | 2.351(2) |
| M–C2 | 1.823(5) | 1.938(6) | 1.829(2) | 1.937(2) |
| M–C3 | 1.810(4) | 1.940(5) | 1.813(2) | 1.928(2) |
| M–C4 | 1.813(5) | 1.928(6) | 1.835(2) | 1.947(2 |
| C2–O1 | 1.173(5) | 1.172(7) | 1.176(3) | 1.172(2) |
| C3–O2 | 1.185(4) | 1.178(6) | 1.168(3) | 1.179(2) |
| C4–O3 | 1.167(5) | 1.181(7) | 1.180(3) | 1.170(2) |
| C1–P1 | 1.624(5) | 1.632(6) | 1.647(2) | 1.647(2) |
| C1–P2 | 1.653(5) | 1.649(6) | 1.646(2) | 1.643(2) |
| P1–C1–P2 | 134.8(2) | 136.2(3) | 129.0(1) | 129.9(1) |

In attempts to crystallize **4a** from DCM/pentane for an extended period of several weeks, a small crop of single crystals of different habitus in comparison to **4a** was separated and analyzed by XRD analysis and IR. The results unveiled a tetracarbonyl complex of the composition [Cr(CO)$_4$(CDP($^{3,5\text{-Me}}$Pz)$_2$)] (**4b**) with one coordinated and one dangling pyrazolyl ligand (Figure 3). Small quantities of **4b** might have formed either upon partial decomposition of **4a** with release of


https://doi.org/10.1021/acs.organomet.1c00231
Organometallics 2021, 40, 2090–2099

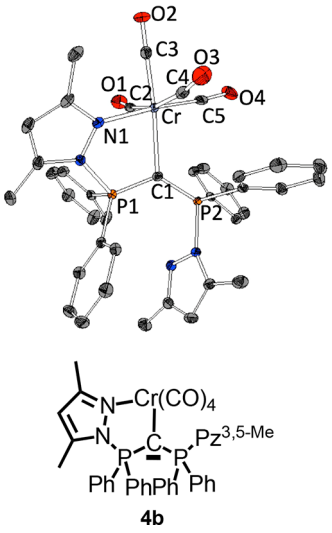


**Figure 3.** Formula and XRD molecular structure of the side or decomposition product *cis*-$[Cr(CO)_4(CDP(^{3,5\text{-}Me}Pz)_2)]$ (**4b**). Hydrogen atoms and solvent molecules have been omitted for clarity; thermal ellipsoids are given at 50% probability. For details see the Supporting Information.

CO or by the presence of traces of $[Cr(CO)_4(MeCN)_2]$ in the $[Cr(CO)_3(MeCN)_3]$ starting material. $[Cr(CO)_4(CDP(^{3,5\text{-}Me}Pz)_2)]$ (**4b**) shows an additional asymmetric stretching vibration due to an additional terminal CO group. Crystallographic data, bond distances, and a DFT analysis of the calculated CO frequencies of **4b** are displayed in Figures S-47, S-48, and S-95 and Table S-4 in the Supporting Information.

The complexes **4**–**9** were investigated via IR spectroscopy. The results of ATR-FT-IR spectra of finely ground solid samples were compared to vibrational spectra in the CO stretching region simulated by DFT calculations (Table 2).

Experimentally, each of the complexes **4**–**9** shows three CO stretching vibrations between 1739 and 1915 $cm^{-1}$. However, the two asymmetric stretching vibrations are superimposed and a shoulder is typically observed. The DFT calculations (PBE-D3(BJ)/def2-TZVPP) support the experimental results and suggest two asymmetric stretching modes between 1829 and 1853 $cm^{-1}$ and one symmetric stretching vibration between 1908 and 1919 $cm^{-1}$.

**Table 2. Calculated and Experimentally Observed C–O Stretching Vibrations of 4–9**[a]

| | wavenumber ($cm^{-1}$) |
|---|---|
| **4a** | |
| calcd | 1829, 1847, 1908 |
| exptl | 1739, 1762, 1884 |
| **5** | |
| calcd | 1835, 1848, 1914 |
| exptl | 1746, 1889 |
| **6** | |
| calcd | 1831, 1847, 1908 |
| exptl | 1746, 1890 |
| **7** | |
| calcd | 1841, 1852, 1913 |
| exptl | 1749, 1774, 1890 |
| **8** | |
| calcd | 1839, 1854, 1919 |
| exptl | 1748, 1777, 1893 |
| **9** | |
| calcd | 1836, 1853, 1914 |
| exptl | 1802, 1868, 1915 |

[a]For more details see Table S-1 and further Supporting Information.

The experimental spectra and corresponding vibrational modes are presented in Figures S-43–S-66 in the Supporting Information. An example of a comparison of the experimental and calculated IR spectra is displayed in Figure S-46.

The calculated vibrations are marginally shifted to higher wavenumbers in comparison to the experimental results. As has already been observed for the N,C,N-CDP complex *fac*-$[Cr(CO)_3(CDP(^2Py)_2)]$,[33] the asymmetric CO stretching vibrations are shifted to lower wavenumbers in comparison to $[Cr(CO)_6]$ (2003 $cm^{-1}$),[44] indicating that the two 3,5-dimethyl-1*H*-pyrazol-1-yl or pyridin-2-yloxy groups are reasonable but less efficient $\pi$-acceptor ligands in comparison to carbonyl groups. In summary, the imidazolyl and pyridyl carbodiphosphoranes **2** and **3** perform as strong C-$\sigma$-donor, medium-strong N-$\sigma$-donor, and weak N-$\pi$-acceptor ligands. The ligand's HOMO, formally the carbone electron pair of $\pi$ symmetry, remains as a nonbonding ligand-centered orbital in these types of carbonyl metal complexes **4**–**9**. This HOMO is partially stabilized by back-bonding into antibonding orbitals of both phosphonio groups, as evidenced by a shorter average P–C bonding distance in comparison to typical P–C single bonds in pentavalent tetracoordinate phosphonium groups such as $Ph_4P^+$ (P–C = 1.799(5) Å).[45]

Our interest in CDP $d^{10}$-Cu(I) complexes arose because compounds of the type $[(CuX)_2(CDP(^2Py)_2)]$ (X = Cl, Br, I) turned out to be fluorescence emitters.[32] For this reason we investigated reactions of **2** and **3** with copper halides CuX. Our attempts to synthesize mononuclear copper(I) complexes of **2** and **3** failed. Instead, dinuclear complexes were isolated in poor yields from equimolar reactions. However, the complexes $[(CuI)_2(CDP(^{3,5\text{-}Me}Pz)_2)]$ (**10**) and $[(CuX)_2(CDP(O\text{-}^2Py)_2)]$ (**11**–**13**, X = Cl, Br, I) were obtained in good yields (66–77%) when **2** or **3** was reacted with 2 equiv of the copper(I) halide in THF (Scheme 3). All of these compounds were obtained as single crystals by layering a solution of the sample in dichloromethane or chloroform with *n*-pentane. Figure 4 displays a selection of two representatives.

$[(CuI)_2(CDP(^{3,5\text{-}Me}Pz)_2)]$ (**10**) crystallizes in triclinic space group *P*$\bar{1}$ with two units in the unit cell. The result of the XRD structure refinements reveals that each of the two ylidic carbon lone pairs bind one trigonally coordinated copper ion of $d^{10}$ electronic configuration. The coordination sphere is complemented by one N donor of the 3,5-dimethyl-1*H*-pyrazol-1-yl ligand and by the iodide ligand. The Cu1–Cu2 distance of 2.543(2) Å is twice the size of the covalent radius of Cu(I) (1.27 Å)[46] and shorter than the van der Waals radius of Cu (1.4 Å).[47] This suggests that a weak metal–metal interaction might complement a distorted quasi-pseudotetrahedral copper coordination sphere. On the other hand, the short Cu–Cu distance can be traced back to this ligand system with two strong geminal Cu–C ylide interactions.[32] On the other hand, the XRD molecular structures of pyridine-2-yloxy-substituted representatives **11**–**13** display much longer distances in the range Cu···Cu 3.266–3.608 Å, which definitely are longer than any strong metal–metal interaction. Obviously, both the type of halide ion and the flexibility of the six-membered in comparison to the more rigid five-membered chelate triggers these $d^{10}$–$d^{10}$ metal distances.


https://doi.org/10.1021/acs.organomet.1c00231
Organometallics 2021, 40, 2090–2099

**Scheme 3. Synthesis of Novel Carbodiphosphorane Copper(I) Complexes of *sym*-Bis(3,5-dimethyl-1*H*-pyrazol-1-yl)carbodiphosphorane (2) and *sym*-Bis(pyridin-2-yloxy)carbodiphosphorane (3)**

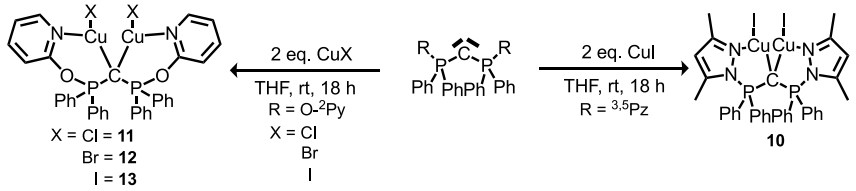


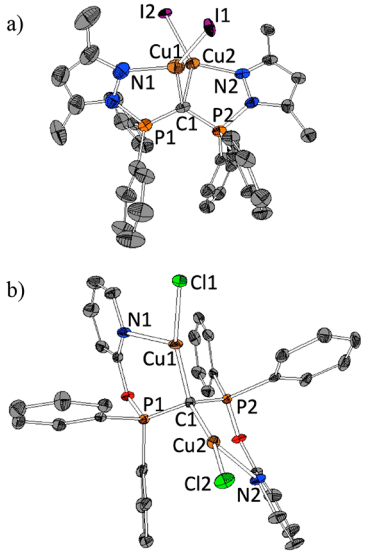


**Figure 4.** XRD molecular structures of the representative dinuclear complexes (a) $[(CuI)_2(CDP(^{3,5\text{-}Me}Pz)_2)]$ (**10**) and (b) $[(CuCl)_2(CDP(O\text{-}^2Py)_2)]$ (**11**). Related analytical results for $[(CuBr)_2(CDP(O\text{-}^2Py)_2)]$ (**12**) and $[(CuI)_2(CDP(O\text{-}^2Py)_2)]$ (**13**) are given in Figure S-82 in the Supporting Information. Hydrogen atoms and solvent molecules have been omitted for clarity; thermal ellipsoids are set at 50% probability.

Complexes **11**−**13** crystallize in the monoclinic space group $P2_1/c$ with two units (**11**) or eight units (**12**, **13**) in their unit cells. Representative distances and angles are presented in Table 3. A noteworthy structural feature is the trend in elongation of both geminal C−CuX bonds with the increasing effective ionic radius of the halide ligand X:[48] namely, Cu1−C1 increases from 1.976(5) Å (**11**) to 1.995(4) Å (**13**) and Cu2−C1 from 1.970(5) Å (**11**) to 2.018(4) Å (**13**). The inverse trend is observed for both N−CuX distances decreasing for Cu1−N1 from 2.297(5) Å (**11**) to 2.199(4) Å (**13**) and for Cu2−N2 from 2.326(4) Å (**11**) to 2.192(3) Å (**13**). These trends reflect the increasing affinity of Cu(I) ions in the order zwitterionic carbon > anionic halide > neutral $sp^2$ nitrogen. The bonds of strongly Cu(I) affine ligands are less influenced by the regime of the other less Cu(I) affine ligands competing for covalent bond shares. The increased electron density of the Cu(I) ions in **11**−**13** can be monitored by NBO analysis. The atomic partial charges $q$(Cu) of the Cu atoms of $[(CuCl)_2(CDP(O\text{-}^2Py)_2)]$ (**11**) are 0.79 and 0.80 e, those of the Cu atoms of $[(CuBr)_2(CDP(O\text{-}^2Py)_2)]$ (**13**) are 0.77 and 0.77 e, and those of the Cu atoms of $[(CuI)_2(CDP(O\text{-}^2Py)_2)]$ (**13**) are 0.74 and 0.74 e.

**Table 3. Selected Bond Distances (Å) and Angles (deg) for 10−13**

| | 10 | 11 | 12[a] | 13[a] |
|---|---|---|---|---|
| Cu1−C1 | 2.061(1) | 1.976(5) | 1.973(6) | 1.995(4) |
| Cu2−C1 | 2.075(1) | 1.970(5) | 1.990(6) | 2.018(4) |
| Cu1−N1 | 2.032(9) | 2.297(5) | 2.254(5) | 2.199(4) |
| Cu2−N2 | 2.028(1) | 2.326(4) | 2.233(6) | 2.192(3) |
| Cu1−X1 | 2.449(1) | 2.164(1) | 2.282(1) | 2.485(3) |
| Cu2−X2 | 2.261(2) | 2.163(2) | 2.282(1) | 2.459(6) |
| Cu1−Cu2 | 2.543(2) | 3.266 | 3.414 | 3.608 |
| C1−P1 | 1.694(1) | 1.691(5) | 1.697(6) | 1.687(4) |
| C1−P2 | 1.688(1) | 1.701(5) | 1.695(6) | 1.695(4) |
| P1−C1−P2 | 120.6(6) | 118.3(3) | 118.7(4) | 119.0(2) |

[a]Only one of the two individual molecules in the unit cell were considered for comparisons. This does not affect the discussed trend. For more information see SI.

The difference in the crystallographic data of **11** ($P2_1/c$, $Z$ = 2) and the related **12** and **13** ($P2_1/c$, Z = 8) has an unexpected reason: much to our surprise, the unit cell of the crystal containing the molecular complex $[(CuCl)_2(CDP(O\text{-}^2Py)_2)]$ (**11**) does contain an independent $[(CuCl)_8(CDP(O\text{-}^2Py)_2)]$ molecule cocrystallizing with **11** in a 1:1 ratio. Its molecular structure is displayed in Figure 5, and selected bonding distances and angles are given in the caption. The cocrystallized product is best rationalized as the eight-membered ring $[Cu_4(\mu_2\text{-}Cl)_4]$ stabilized by two Cu,Cu′-bridging neutral Cl,Cl′-donor ligands **11** and $[3(CuCl)_2]$, respectively (see Figure 5). It seems that the bite of electron-rich terminal chlorido functionalities in molecular **11** perfectly fits the

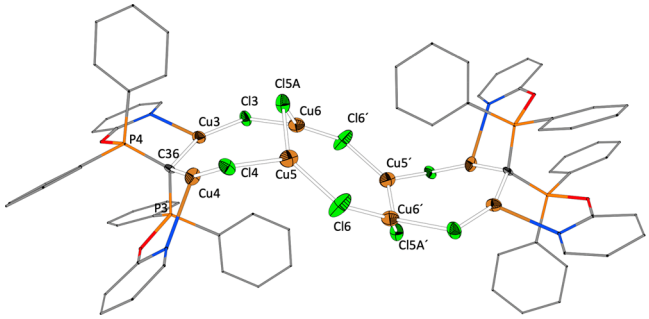


**Figure 5.** X-ray crystal structure of $[(CuCl)_8(CDP(O\text{-}^2Py)_2)_2]$ cocrystallized with $[(CuCl)_2(CDP(O\text{-}^2Py)_2)]$ (**11**). Hydrogen atoms and solvent molecules have been omitted for clarity; thermal ellipsoids are given at 50% probability. For details see the Supporting Information. Bond lengths (Å): P3−C36 1.698(5), P4−C36 1.703(5), C36−Cu3 1.957(5), C36−Cu4 1.985(5), Cl3−Cu6 2.394(2), Cl4−Cu5 2.315(2), Cu5−Cl5A 2.226(3), Cu5−Cl6 2.196(2), Cu6−Cl5A 2.215(3), Cu6−Cl6′ 2.203(2). Bond angles (deg): P3−C36−P4 118.3(3), Cu3−C36−Cu4 119.4(3), C36−Cu3−Cl3 163.9(2), C36−Cu4−Cl4 157.6(2), Cu3−Cl3−Cu6 85.3(6), Cu4−Cl4−Cu5 100.4(7), Cu5−Cl6−Cu6 127.0(9), Cu5−Cl5A−Cu6 107.3(1).



https://doi.org/10.1021/acs.organomet.1c00231
Organometallics 2021, 40, 2090−2099

stabilization of each copper atom of the supramolecular 8-ring array $[Cu_4(\mu_2\text{-}Cl)_4]$ by 2 × 2 dative (**3**)Cu−Cl→Cu bonds. This interaction leads to more or less trigonally coordinated $d^{10}$-Cu(I) ions of coordination number 3 and to Cl−Cu−Cl angles, allowing the central eight-membered ring structure to be built up in a chair conformation. It is plausible that this supermolecule of composition $[(CuCl)_8(CDP(O\text{-}^2Py)_2)_2]$ had formed upon the reaction of molecular complex **11** with an excess of $[CuCl]_x$.

The structural chemistry of Lewis base adducts of $[CuCl]_x$ is extraordinarily rich. Similar $[Cu_4(\mu_2\text{-}Cl)_4]$ cores can exist either in a "tube" form[49−52] or in a "step" or "twist-chair" form.[53−57] Some of the latter forms exist with two linear and collinear Cl−Cu−Cl units with angles close to 180°.[58−62] The eight-membered $Cu_4Cl_4$ unit can be part of a "drumlike" $Cu_6X_6$ unit.[63] In $[(CuCl)_8(CDP(O\text{-}^2Py)_2)_2]$ the central $Cu_4Cl_4$ core reveals an unusual motif with a plane defined by six atoms (4 × Cu and 2 × Cl: Cu5, Cu5′, Cu6, Cu6′ and Cl6, Cl6′) and only two out-of-plane chloride ions Cl5 and Cl5′. The out-of-plane chloride ions are formally induced by two neutral copper-bridging Cl,Cl′-ligands **11**.

Furthermore, the series of Cu(I) halide complexes **11**−**13** of $CDP(O\text{-}^2Py)_2$ (**3**) were analyzed using UV/vis spectroscopy. The presence of an electron-rich oxa group at the pyridine functionality seems to quench photoluminescence (PL). **11**−**13** are PL-silent in contrast to corresponding PL-active Cu(I) halide complexes of $CDP(^2Py)_2$ with its pyridine-centered LUMO of low energy.[32] Table 4 summarizes the absorption maxima and the extinction coefficients; correlated spectra are displayed in Figure 6.

**Table 4. Absorption Maxima and Extinction Coefficients of 3 and the Corresponding Complexes 11−13**

| | $\lambda_{max}$ (nm) | $\varepsilon$ (L mol$^{-1}$ cm$^{-1}$) |
|---|---|---|
| **3** | 306 | $2.415 \times 10^3$ |
| **11** | 263 | $1.069 \times 10^4$ |
| **12** | 278 | $5.920 \times 10^3$ |
| **13** | 277 | $8.511 \times 10^3$ |

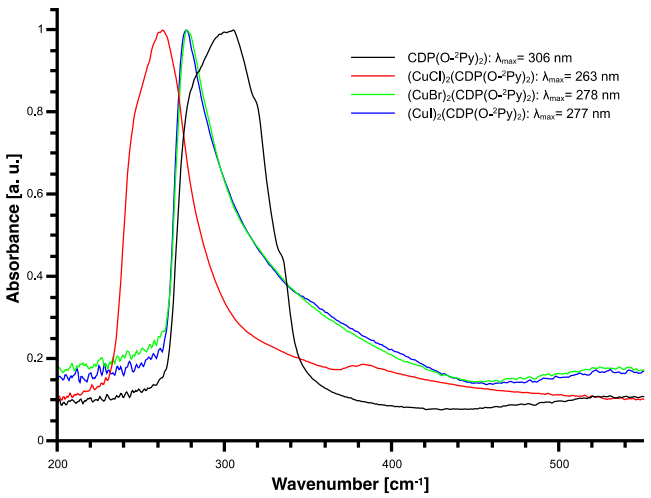


**Figure 6.** Experimental UV/vis spectrum of $(CDP(O\text{-}^2Py)_2)$ (**3**, black) and the corresponding complexes **11** (red), **12** (green), and **13** (blue).

While ligand **3** shows an absorption maximum at 306 nm with an extinction coefficient of $2.415 \times 10^3$ L mol$^{-1}$ cm$^{-1}$, the copper complexes display a significant shift to lower wavelengths: **12** and **13** exhibit nearly the same shape and maxima at 278 and 277 nm, and chloride complex **11** is even further shifted to lower wavelengths (263 nm).

In order to gain a better understanding of redox processes, the representative complex $[(CuI)_2(CDP(O\text{-}^2Py)_2)]$ (**13**) was studied via cyclic voltammetry versus ferrocene in DMSO at room temperature ($c$ = 5.153 mmol/L, scan rate 100 mV/s). The CV plot is displayed in Figure 7, and redox potentials are

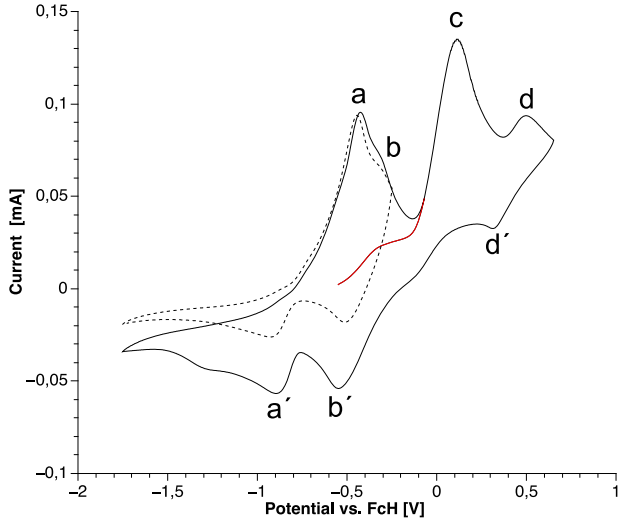


**Figure 7.** Plots of the cyclic voltammetry of $[(CuI)_2(CDP(O\text{-}^2Py)_2)]$ (**13**) in DMSO at room temperature ($c$ = 5.153 mmol/L) with $TBAPF_6$ (50 mmol/L) as electrolyte at a scan rate of 100 mV/s. The red line shows the first cycle. Potentials are plotted against the ferrocene/ferrocenium redox couple. A platinum working electrode (diameter 0.25 mm) and a platinum counter electrode were used, as well as a silver/silver sulfide reference electrode. The dashed line shows the plot with a switching potential of −0.25 V.

**Table 5. Redox Processes Observed in the CV of $[(CuI)_2(CDP(O\text{-}^2Py)_2)]$ (13)**

| oxidation process | oxidation potential (V) |
|---|---|
| a | −0.43 |
| b | |
| c | 0.14 |
| d | 0.50 |
| **reduction process** | **reduction potential (V)** |
| a′ | −0.89 |
| b′ | −0.55 |
| d′ | 0.31 |

given in Table 5. The plot shows four oxidation potentials in the anodic section of the cyclic voltammogram: a−d. At the same time only three corresponding redox couples are observed in the cathodic part of the spectrum, which can be assigned to the oxidation potentials a′, b′, and d′. Oxidation process c is an irreversible process. The red line of the CV plot of $[(CuI)_2(CDP(O\text{-}^2Py)_2)]$ (**13**) describes the first cycle of the measurement. With a starting voltage of −0.50 V the formation of the peaks a and b cannot be observed unless they undergo the reduction processes a′ and b′.


https://doi.org/10.1021/acs.organomet.1c00231
Organometallics 2021, 40, 2090−2099

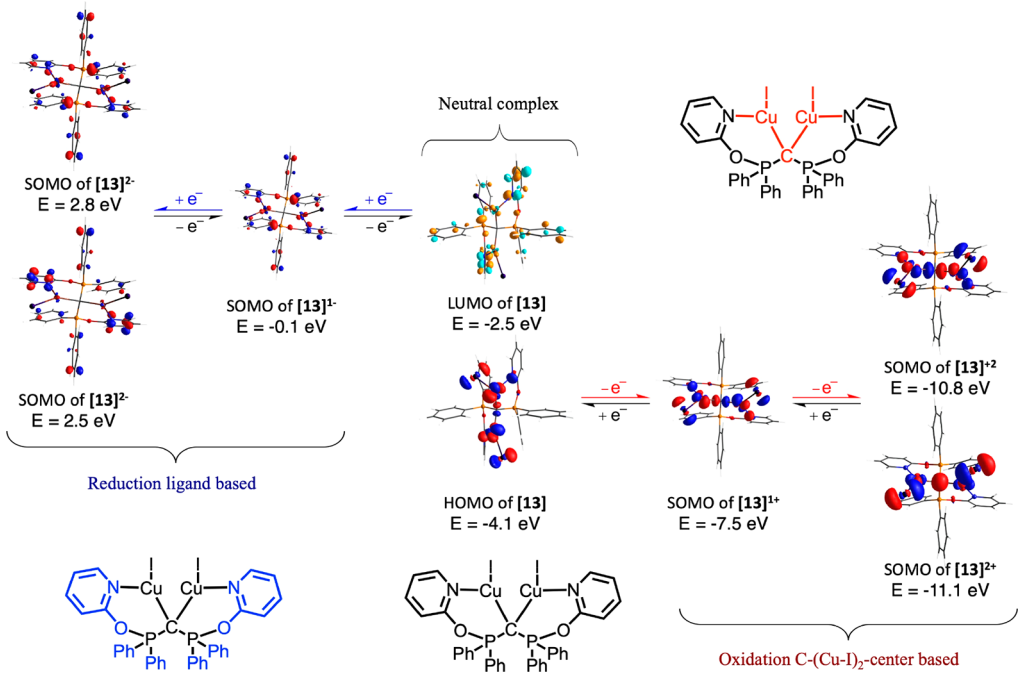


**Figure 8.** Redox processes of $[(CuI)_2(CDP(O\text{-}^2Py)_2)]$ (**13**) simulated via DFT calculations and the corresponding Kohn−Sham orbitals (isovalue 0.05). Calculations were performed at the PBE-D3(BJ)/def2-TZVPP level of theory. In the case of $[\mathbf{13}]^{2-}$ and $[\mathbf{13}]^{2+}$ the triplet states lower in energy in comparison to singlet states are presented. The blue/red color code in the formula **13** indicates where oxidation (red) and reduction (blue) take place. The turquoise/orange coding represents unoccupied and red/blue coding illustrates occupied Kohn−Sham orbitals.

The processes a/a′ and b/b′ were further investigated individually by reducing the switching potential to −0.25 V (dashed line in Figure 7). In this case the reaction can tentatively be considered as a quasi-reversible two-electron-ransfer process. On consideration that at the start of the cycle only the neutral compound **13** is present, both processes can be considered as reversible reduction waves of **13** forming $[\mathbf{13}]^{2-}$. In the following oxidation cycle $[\mathbf{13}]^{2-}$ is reoxidized to the neutral species **13**. Therefore, a can be considered as the oxidizing process $[\mathbf{13}]^{2-} \rightarrow [\mathbf{13}]^{-}$ and a′ as the reducing process $[\mathbf{13}]^{-} \rightarrow [\mathbf{13}]^{2-}$, while b is the inverse $[\mathbf{13}]^{-} \rightarrow \mathbf{13}$ and b′ is $\mathbf{13} \rightarrow [\mathbf{13}]^{-}$. This leads to the conclusion that the reaction can be considered as a quasi-reversible redox reaction in the potential range of −1.75 to −0.25 V. In the extended range −1.75 to +0.75 V, the an oxidation process c is observed followed by another oxidation d. While d shows a corresponding reduction process d′, c does not show a corresponding reduction process and seems to be irreversible.

In order to gain a deeper understanding of these redox processes, the frontier orbitals of **13** were calculated using DFT at the PBE-D3(BJ)/def2-TZVPP level of theory. The results are displayed in Figure 8 (see also Figure S-78). The DFT calculations reveal that the electron density of HOMO and HOMO-1 is delocalized over seven atoms of both copper atoms and their direct donor atoms: the central ylidic C atom as well as the two Cu−I units, and to a smaller extent both $sp^2$ N donor atoms. At the same time the LUMO and LUMO+1 can be considered as being ligand based, located mainly at both phosphino groups including their aryl carbon backbone with a higher population at the pyridyl groups. On consideration that oxidation takes place at the HOMO and reductive electron transfer occurs into the LUMO, the calculations suggest that the redox processes a/a′ and b/b′ refer to ligand-based processes, which are typical for noninnocent ligands.[64] When it is taken into account that the stepwise reduction of **13** addresses the LUMO, a singly occupied molecular orbital (SOMO) with a duplet character (Figure 8) is formed. This reduction reaction $\mathbf{13} \rightarrow [\mathbf{13}]^{-}$ refers to process **b**′ in the CV experiment. Once again, the SOMO is mainly of ligand character and is located on the phenyl and pyridyl groups and not at copper. By further reduction of $[\mathbf{13}]^{-}$ to $[\mathbf{13}]^{2-}$ either a singlet or a triplet state can be formed. The calculations show that the triplet state is energetically slightly more stable; therefore, two SOMOs are formed. Both SOMOs are strongly phenyl and pyridyl based and also show only a very small contribution of both copper atoms. This process can be related to process a′ and describes $[\mathbf{13}]^{-} \rightarrow [\mathbf{13}]^{2-}$. The experimental results of the CV measurements suggest that these reductions are reversible. On the other hand, the oxidation seems to be irreversible. As was mentioned, the HOMO is spread over the central $C-(Cu-I)_2-N^{py}_2$ unit. An oxidation leads to $[\mathbf{13}]^{+}$, where the positive charge is equally spread all over this seven-atom unit. This can be illustrated by the duplet character of SOMO of $[\mathbf{13}]^{+}$ that is formed (Figure 8). As the SOMO shows high symmetry, the existence of the mixed-valent $[(Cu^{II}I)(Cu^{I}I)(CDP(O\text{-}^2Py)_2)]^{+}$ is unlikely. This consideration is supported by an NBO analysis, where the natural charges of the copper atoms are almost equal: $q(Cu1) = 0.85$ e and $q(Cu2) = 0.85$ e. Further oxidation of $[\mathbf{13}]^{+} \rightarrow [\mathbf{13}]^{2+}$ generates a triplet state with two SOMOs; the corresponding singlet state is 53.6 kJ/mol less favorable. While the energetically marginally lower lying SOMO displays a strong $C-(Cu-I)_2$ character, the Kohn−Sham orbitals of the second SOMO are spread over the complete $C-(Cu-I)_2-N^{py}_2$ unit. Therefore, the oxidation processes can be considered as electron transfer occurring not only from both Cu(I) metal centers but also as a process that affects the whole $C-(Cu-I)_2-N^{py}_2$ unit. This complicates a distinct interpretation of the


https://doi.org/10.1021/acs.organomet.1c00231
Organometallics 2021, 40, 2090−2099

processes c, d, and d′ of the CV measurements. Additionally, we have to consider that the calculations evaluate the gas-phase environment and that the solvent DMSO used in CV should have an effect upon oxidizing the neutral compound **13** to a cation and dication. A summation of both the calculations and CV measurements suggests that ligand **3** can act as a noninnocent ligand and the redox behavior can be considered as quasi-reversible in the potential range of −1.75 to −0.25 V. This feature is of interest for designing transition-metal complexes or catalysts with potentially redox active sites.

## CONCLUSION

A new generation of carbodiphosphoranes incorporating two chelating N-donor functionalities was introduced. A novel synthesis strategy, the reaction of P-electrophile CDP-$Cl_2$ (**1**) with ambident pyrazolate and 2-pyridinolate anions, has been established in order to isolate *sym*-bis(3,5-dimethyl-1*H*-pyrazol-1-yl)carbodiphosphorane $CDP(^{3,5\text{-Me}}Pz)_2$ (**2**) and *sym*-bis(pyridin-2-yloxy)carbodiphosphorane $CDP(O\text{-}^2Py)_2$ (**3**) in their free ligand base forms. In contrast to N,C,N pincer ligands incorporating a central NHC carbon donor, neutral CDP ligands **2** and **3** are more flexible, both in the number of donated electrons of their zwitterionic carbon atom, a $\sigma$-, $\sigma,\pi$- or $2\sigma$-electron pair donor, and in their ability to adapt to M−L configurations other than only meridional: e.g., also facial. For a first insight into their coordination capability, we chose $d^6$-$[M(CO)_3]$ fragments (M = Cr, Mo, W) forming octahedral complexes of the type *fac*-$[M(CO)_3(CDP(^{3,5\text{-Me}}Pz)_2)]$ (**4**−**6**) and *fac*-$[M(CO)_3(CDP(O\text{-}^2Py)_2)]$ (**7**−**9**) and $d^{10}$-[CuX] fragments (X = Cl, Br, I) forming dinuclear complexes $[(CuI)_2(CDP(^{3,5\text{-Me}}Pz)_2)]$ (**10**) and $[(CuX)_2(CDP(O\text{-}^2Py)_2)]$ (**11**−**13**) next to the unexpected cocrystallized octanuclear supramolecular complex $[(CuCl)_8(CDP(O\text{-}^2Py)_2)]$. The characterization focused on XRD, IR, and UV−vis studies. The ligand properties, vibrational modes of the carbonyl complexes, and electroanalytical results of a representative CV of **13** were modeled by DFT calculations.

## EXPERIMENTAL SECTION

**General Considerations.** Reactions were carried out under an inert atmosphere using standard Schlenk techniques. Moisture- and air-sensitive substances were stored in a conventional nitrogen-flushed glovebox. *sym*-Bis(*P*-chlorodiphenyl)carbodiphosphorane (**1**) was synthesized via a modified procedure adapted from Appel et al.[37] Details of this modification, of all synthetic procedures, analyses, and characterizations, of DFT calculations, and of analytical and spectroscopic instruments used are given in the Supporting Information.

**Ligand Syntheses and Characterization.** *Bis(3,5-dimethyl-1H-pyrazol-1-yl)carbodiphosphorane (2).* A 3.00 g portion of **1** (6.62 mmol, 1.00 equiv) and 1.77 g of potassium 3,5-dimethyl-1*H*-pyrazol-1-yl (13.2 mmol, 2.00 equiv), prepared from KH and 3,5-dimethylpyrazole in THF, were suspended in 50 mL of THF at −78 °C and stirred for 18 h while the mixture was warmed to rt. The solvent was removed under reduced pressure, and the residue was washed with DEE (2 × 10 mL) and with *n*-pentane (2 × 10 mL) and dried under reduced pressure ($1 \times 10^{-3}$ mbar) to form the desired product **2** as a light green powder (2.93 g, 5.01 mmol, 77%). $^{31}P\{^1H\}$ NMR (101 MHz, $C_6D_6$): $\delta$/ppm 8.9 (s). $^1H$ NMR (300 MHz, $C_6D_6$): $\delta$/ppm 7.92.7.84 (m, 8 H, $H_2$), 7.05−6.98 (m, 12 H, $H_3$/ $H_4$), 5.58 (s, 2H, $H_5$), 2.29 (s, 6H, $H_7$), 2.09 (s, 6H, $H_6$). $^{13}C\{^1H\}$ NMR (75 MHz, $C_6D_6$): $\delta$/ppm 149.7, 146.8, 136.7, 135.9, 135.1, 132.7, 130.3, 109.2, 13.9. APCI$^+$/HRMS ($CH_2Cl_2$) *m*/*z* (%) calcd for $[C_{35}H_{34}P_2N_4]H^+$ 573.2337, found 573.2323.

*Bis(pyridin-2-yloxy)carbodiphosphorane (3).* A 2.00 g portion of **1** (4.41 mmol, 1.00 equiv) and 1.03 g of sodium-2-pyridinolate (8.83 mmol, 2.00 equiv), prepared from 2-hydroxypyridine and NaH in THF, were suspended in 15 mL of THF and stirred for 18 h at rt. The solvent was removed under reduced pressure, and the residue was washed with DEE (2 × 10 mL) and with *n*-pentane (2 × 10 mL) and dried under reduced pressure ($1 \times 10^{-3}$ mbar) to form the desired product **3** as a gray powder (2.69 g, 4.41 mmol, quantitative). $^{31}P\{^1H\}$ NMR (101 MHz, $CD_2Cl_2$): $\delta$/ppm 23.1 (s). $^1H$ NMR (300 MHz, $CD_2Cl_2$): $\delta$/ppm 8.05 (dd, $^{3,5}J_{H,H}$ = 2.1, 4.3 Hz, 2 H, $H_1$), 7.82−7.72 (m, 8 H, $H_7$), 7.41−7.19 (m, 14 H, $H_3$/$H_8$/$H_9$), 6.92−6.84 (m, 4 H, $H_2$/$H_4$). $^{13}C\{^1H\}$ NMR (75 MHz, $CD_2Cl_2$): $\delta$/ppm 148.1 (s, $C_1$), 138.7 (s, $C_3$), 131.9 (t, $J_{C,P}$ = 5.6 Hz, $C_7$), 130.4 (s, $C_9$), 128.2 (t, $J_{C,P}$ = 6.8 Hz, $C_8$), 119.5 (s, $C_2$), 115.7 (s, $C_4$). APCI$^+$/HRMS ($CH_2Cl_2$): *m*/*z* (%) calcd for $[C_{35}H_{28}P_2O_2N_2]H^+$ 571.1704, found 517.1702. UV/vis ($CH_2Cl_2$): *c* = 169.1 $\mu$m, $\lambda_{max}$ = 306 nm, $\varepsilon = 2.415 \times 10^3$ L mol$^{-1}$ cm$^{-1}$.

## ASSOCIATED CONTENT

### Supporting Information

The Supporting Information is available free of charge at https://pubs.acs.org/doi/10.1021/acs.organomet.1c00231.

Experimental procedures, IR spectra, UV/vis spectra, CV measurements, elemental analysis results, crystal data tables, and details and results of DFT calculations (PDF)

Cartesian coordinates of calculated structures (XYZ)

### Accession Codes

CCDC 1976467, 1976473, 1976475, 1976477−1976478, and 1976486−1976489 contain the supplementary crystallographic data for this paper. These data can be obtained free of charge via www.ccdc.cam.ac.uk/data_request/cif, or by emailing data_request@ccdc.cam.ac.uk, or by contacting The Cambridge Crystallographic Data Centre, 12 Union Road, Cambridge CB2 1EZ, UK; fax: +44 1223 336033.

## AUTHOR INFORMATION


### Corresponding Author

**Jörg Sundermeyer** − *Fachbereich Chemie and Wissenschaftliches Zentrum für Materialwissenschaften, Philipps-Universität Marburg, 35043 Marburg, Germany;* orcid.org/0000-0001-8244-8201; Email: jsu@staff.uni-marburg.de

### Author

**Marius Klein** − *Fachbereich Chemie and Wissenschaftliches Zentrum für Materialwissenschaften, Philipps-Universität Marburg, 35043 Marburg, Germany*

Complete contact information is available at: https://pubs.acs.org/10.1021/acs.organomet.1c00231


### Notes

The authors declare no competing financial interest.

## REFERENCES


(1) Ramirez, F.; Desai, N. B.; Hansen, B.; McKelvie, N. Hexaphenylcarbodiphosphorane, $(C_6H_5)_3PCP(C_6H_5)_3$. *J. Am. Chem. Soc.* **1961**, *83* (16), 3539−3540.

(2) Petz, W.; Frenking, G. Carbodiphosphoranes and Related Ligands. In *Transition Metal Complexes of Neutral $\eta^1$-Carbon Ligands*; Springer-Verlag: Berlin, 2010; Vol. *30*, pp 49−92.

(3) Petz, W. Addition Compounds between Carbones, $CL_2$, and Main Group Lewis Acids: A New Glance at Old and New Compounds. *Coord. Chem. Rev.* **2015**, *291*, 1−27.

(4) Gessner, V. H. *Modern Ylide Chemistry*; Gessner, V. H., Ed.; Springer International: Oxford, United Kingdom, 2018.
(5) Zhao, L.; Chai, C.; Petz, W.; Frenking, G. Carbones and Carbon Atom as Ligands in Transition Metal Complexes. *Molecules* **2020**, *25*, 4943.
(6) Tonner, R.; Frenking, G. Divalent Carbon(0) Chemistry, Part 1: Parent Compounds. *Chem. - Eur. J.* **2008**, *14* (11), 3260−3272.
(7) Tonner, R.; Frenking, G. Divalent Carbon(0) Chemistry, Part 2: Protonation and Complexes with Main Group and Transition Metal Lewis Acids. *Chem. - Eur. J.* **2008**, *14* (11), 3273−3289.
(8) Tonner, R.; Frenking, G. $C(NHC)_2$: Divalent Carbon(0) Compounds with N-Heterocyclic Carbene Ligands—Theoretical Evidence for a Class of Molecules with Promising Chemical Properties. *Angew. Chem., Int. Ed.* **2007**, *46* (45), 8695−8698.
(9) Frenking, G.; Tonner, R. Divalent Carbon(0) Compounds. *Pure Appl. Chem.* **2009**, *81* (4), 597−614.
(10) Tonner, R.; Öxler, F.; Neumüller, B.; Petz, W.; Frenking, G. Carbodiphosphoranes: The Chemistry of Divalent Carbon(0). *Angew. Chem., Int. Ed.* **2006**, *45* (47), 8038−8042.
(11) Appel, R.; Knoll, F.; Schöler, H.; Wihler, H.-D. Vereinfachte Synthese von Bis(triphenylphosphoranyliden)methan. *Angew. Chem.* **1976**, *88* (22), 769−770.
(12) (a) Sundermeyer, J.; Weber, K.; Peters, K.; von Schnering, H. G. Modeling Surface Reactivity of Metal Oxides: Synthesis and Structure of an Ionic Organorhenyl Perrhenate Formed by Ligand-Induced Dissociation of Covalent $Re_2O_7$. *Organometallics* **1994**, *13*, 2560−2562. (b) Pikl, R.; Weber, K.; Sundermeyer, J.; Herrmann, W. A.; Kiefer, W. Vibrational study on rhenium oxo complexes: Normal coordinate analysis of $H_3C$-$ReO_3$ and $[L\text{-}ReO_3]^+$ {L = $Ph_3P{=}C{=}PPh_3$}. *Vib. Spectrosc.* **1997**, *14*, 299−302.
(13) Driscoll, J. S.; Grisley, D. W.; Pustinger, J. V.; Harris, J. E.; Matthews, C. N. Properties and Reactions of Mesomeric Phosphonium Salts1. *J. Org. Chem.* **1964**, *29* (8), 2427−2431.
(14) Zybill, C.; Mueller, G. Mononuclear Complexes of Copper(I) and Silver(I) Featuring the Metals Exclusively Bound to Carbon. Synthesis and Structure of ($^5$-Pentamethylcyclopentadienyl)-[(triphenylphosphonio)(triphenylphosphoranylidene)methyl]-Copper(I). *Organometallics* **1987**, *6* (12), 2489−2494.
(15) Appel, R.; Baumeister, U.; Knoch, F. Darstellung und Molekülstruktur aminosubstituierter Carbodiphosphorane. *Chem. Ber.* **1983**, *116* (6), 2275−2284.
(16) Appel, R.; Morse, G. J. Methanetetraylbis(phosphoranes) (Carbodiphosphoranes). *Inorg. Synth.* **2007**, *24* (36), 113−117.
(17) Kubo, K.; Jones, N. D.; Ferguson, M. J.; McDonald, R.; Cavell, R. G. Chelate and Pincer Carbene Complexes of Rhodium and Platinum Derived from Hexaphenylcarbodiphosphorane, $Ph_3PCPPh_3$. *J. Am. Chem. Soc.* **2005**, *127* (15), 5314−5315.
(18) Cavell, R. G. *Pincer and Chelate Carbodiphosphorane Complexes of Noble Metals*; Morales-Morales, D., Jensen, C., Eds.; Elsevier Science: Amsterdam, 2007; Chapter 15, pp 347−355.
(19) Kubo, K.; Okitsu, H.; Miwa, H.; Kume, S.; Cavell, R. G.; Mizuta, T. Carbon(0)-Bridged Pt/Ag Dinuclear and Tetranuclear Complexes Based on a Cyclometalated Pincer Carbodiphosphorane Platform. *Organometallics* **2017**, *36* (2), 266−274.
(20) Petz, W.; Neumüller, B.; Klein, S.; Frenking, G. Syntheses and Crystal Structures of $[Hg\{C(PPh_3)_2\}_2][Hg_2I_6]$ and $[Cu\{C(PPh_3)_2\}_2]$ I and Comparative Theoretical Study of Carbene Complexes $[M(NHC)_2]$ with Carbone Complexes $[M\{C(PH_3)_2\}_2]$ (M = $Cu^+$, $Ag^+$, $Au^+$, $Zn^{2+}$, $Cd^{2+}$, $Hg^{2+}$). *Organometallics* **2011**, *30* (12), 3330−3339.
(21) Petz, W.; Neumüller, B. New Platinum Complexes with Carbodiphosphorane as Pincer Ligand via Ortho Phenyl Metallation. *Polyhedron* **2011**, *30* (11), 1779−1784.
(22) Buchner, M. R.; Pan, S.; Poggel, C.; Spang, N.; Müller, M.; Frenking, G.; Sundermeyer, J. Di-Ortho-Beryllated Carbodiphosphorane: A Compound with a Metal−Carbon Double Bond to an Element of the s-Block. *Organometallics* **2020**, *39* (17), 3224−3231.
(23) Bottger, S. C.; Poggel, C.; Sundermeyer, J. Ortho-Directed Dilithiation of Hexaphenyl-Carbodiphosphorane. *Organometallics* **2020**, *39*, 3789−3793.
(24) Stallinger, S.; Reitsamer, C.; Schuh, W.; Kopacka, H.; Wurst, K.; Peringer, P. Novel Route to Carbodiphosphoranes Producing a New P,C,P Pincer Carbene Ligand. *Chem. Commun.* **2007**, 510−512.
(25) Reitsamer, C.; Schuh, W.; Kopacka, H.; Wurst, K.; Peringer, P. Synthesis and Structure of the First Heterodinuclear PCP−Pincer−CDP Complex with a Pd−Au $d^8$−$d^{10}$ Pseudo-Closed-Shell Interaction. *Organometallics* **2009**, *28* (22), 6617−6620.
(26) Reitsamer, C.; Schuh, W.; Kopacka, H.; Wurst, K.; Ellmerer, E. P.; Peringer, P. The First Carbodiphosphorane Complex with Two Palladium Centers Attached to the CDP Carbon: Assembly of a Single-Stranded di-Pd Helicate by the PCP Pincer Ligand $C(dppm)_2$. *Organometallics* **2011**, *30* (15), 4220−4223.
(27) Reitsamer, C.; Stallinger, S.; Schuh, W.; Kopacka, H.; Wurst, K.; Obendorf, D.; Peringer, P. Novel Access to Carbodiphosphoranes in the Coordination Sphere of Group 10 Metals: Template Synthesis and Protonation of PCP Pincer Carbodiphosphorane Complexes of $C(dppm)_2$. *Dalton Trans.* **2012**, *41* (12), 3503−3514.
(28) Reitsamer, C.; Hackl, I.; Schuh, W.; Kopacka, H.; Wurst, K.; Peringer, P. Gold(I) and Gold(III) Complexes of the $[CH(dppm)_2]^+$ and $C(dppm)_2$ PCP Pincer Ligand Systems. *J. Organomet. Chem.* **2017**, *830*, 150−154.
(29) Maser, L.; Herritsch, J.; Langer, R. Carbodiphosphorane-Based Nickel Pincer Complexes and Their (de)Protonated Analogues: Dimerisation, Ligand Tautomers and Proton Affinities. *Dalton Trans.* **2018**, *47* (31), 10544−10552.
(30) Maser, L.; Vondung, L.; Langer, R. The ABC in Pincer Chemistry − From Amine- to Borylene- and Carbon-Based Pincer-Ligands. *Polyhedron* **2018**, *143*, 28−42.
(31) Xu, W.; Maser, L.; Alig, L.; Langer, R. Rhodium Carbonyl Complexes Featuring Carbodiphosphorane-Based Pincer Ligands. *Polyhedron* **2021**, *196*, 115018.
(32) Klein, M.; Demirel, N.; Schinabeck, A.; Yersin, H.; Sundermeyer, J. Cu(I) Complexes of a *N,C,N*- and a *P,C,P*-Carbodiphosphorane Ligand. *Molecules* **2020**, *25* (17), 3990−1−15.
(33) Klein, M.; Xie, X.; Burghaus, O.; Sundermeyer, J. Synthesis and Characterization of a *N,C,N*-Carbodiphosphorane Pincer Ligand and Its Complexes. *Organometallics* **2019**, *38* (19), 3768−3777.
(34) (a) Su, W.; Pan, S.; Sun, X.; Zhao, L.; Frenking, G.; Zhu, C. Cerium−Carbon Dative Interactions Supported by Carbodiphosphorane. *Dalton Trans.* **2019**, *48* (42), 16108−16114. (b) Su, W.; Pan, S.; Sun, X.; Wang, S.; Zhao, L.; Frenking, G.; Zhu, C. Double Dative Bond between Divalent Carbon(0) and Uranium. *Nat. Commun.* **2018**, *9*, 4997−5004.
(35) Alcarazo, M.; Radkowski, K.; Mehler, G.; Goddard, R.; Fürstner, A. Chiral Heterobimetallic Complexes of Carbodiphosphoranes and Phosphinidene-Carbene Adducts. *Chem. Commun.* **2013**, *49* (30), 3140−3142.
(36) (a) Kroll, A.; Steinert, H.; Scharf, L. T.; Scherpf, T.; Mallick, B.; Gessner, V. H. A Diamino-Substituted Carbodiphosphorane as Strong C-Donor and Weak N-Donor: Isolation of Monomeric Trigonal-Planar L·$ZnCl_2$. *Chem. Commun.* **2020**, *56* (58), 8051−8054. (b) Ullrich, S.; Kovacevic, B.; Koch, B.; Harms, K.; Sundermeyer, J. Design of non-ionic carbon superbases: second generation carbodiphosphoranes. *Chemical Science* **2019**, *10*, 9483−9492.
(37) Appel, R.; Waid, K. Bis(chlorophenylphosphoranediyl)-methane. *Angew. Chem., Int. Ed. Engl.* **1979**, *18* (2), 169.
(38) Hardy, G. E.; Zink, J. I.; Kaska, W. C.; Baldwin, J. C. Structure and Triboluminescence of Polymorphs of Hexaphenylcarbodiphosphorane. *J. Am. Chem. Soc.* **1978**, *100* (25), 8001−8002.
(39) Birum, G. H.; Matthews, C. N. Mesomeric Phosphonium Dications. *J. Am. Chem. Soc.* **1966**, *88* (18), 4198−4203.
(40) Fluck, E.; Neumüller, B.; Braun, R.; Heckmann, G.; Simon, A.; Borrmann, H. Fluor-Substituierte und andere neue Carbodiphosphorane. *Z. Anorg. Allg. Chem.* **1988**, *567* (1), 23−38.


https://doi.org/10.1021/acs.organomet.1c00231
*Organometallics* 2021, 40, 2090−2099

(41) Vincent, A. T.; Wheatley, P. J. Crystal Structure of Bis(triphenylphosphoranylidene)methane [Hexaphenylcarbodiphosphorane, $Ph_3P{=}C{=}PPh_3$]. *Dalton Trans.* **1972**, 617−622.
(42) Böttger, S.; Gruber, M.; Münzer, J. E.; Bernard, G. M.; Kneusels, N.-J. H.; Poggel, C.; Klein, M.; Hampel, F.; Neumüller, B.; Sundermeyer, J.; Michaelis, V. K.; Tonner, R.; Tykwinski, R. R.; Kuzu, I. Solvent Induced Bond-Bending Isomerism in Hexaphenyl Carbodiphosphorane − Decisive Dispersion Interactions in the Solid State. *Inorg. Chem.* **2020**, *59* (17), 12054−12064.
(43) Cordero, B.; Gómez, V.; Platero-Prats, A. E.; Revés, M.; Echeverría, J.; Cremades, E.; Barragán, F.; Alvarez, S. Covalent Radii Revisited. *Dalton Trans.* **2008**, 2832−2838.
(44) Brathwaite, A. D.; Reed, Z. D.; Duncan, M. A. Infrared Photodissociation Spectroscopy of Copper Carbonyl Cations. *J. Phys. Chem. A* **2011**, *115* (38), 10461−10469.
(45) Minkwitz, R.; Berkei, M.; Ludwig, R. Preparation and Crystal Structure of Tetraphenylphosphonium Triiodotetrabromide $[PPh_4][I_3Br_4]$. *Inorg. Chem.* **2001**, *40* (1), 25−28.
(46) Soloveichik, G. L.; Eisenstein, O.; Poulton, J. T.; Streib, W. E.; Huffman, J. C.; Caulton, K. G. Multiple Structural Variants of $L_nCu^I(\mu\text{-}X)_2Cu^IL_n$ (n = 1, 2). Influence of Halide on a "Soft" Potential Energy Surface. *Inorg. Chem.* **1992**, *31* (15), 3306−3312.
(47) Bondi, A. Van Der Waals Volumes and Radii. *J. Phys. Chem.* **1964**, *68* (3), 441−451.
(48) Shannon, R. D. Revised Effective Ionic Radii and Systematic Studies of Interatomic Distances in Halides and Chalcogenides. *Acta Crystallogr., Sect. A: Cryst. Phys., Diffr., Theor. Gen. Crystallogr.* **1976**, *32* (5), 751−767.
(49) Zhao, Y.; Zhou, Y.; Chen, T.; Yin, S.-F.; Han, L.-B. Synthesis and Molecular Structure of Tetranuclear $Cu_4P_4$ Complexes with $R_2P{-}O{-}PR_2$ Ligands. *Inorg. Chim. Acta* **2014**, *422*, 36−39.
(50) Baenziger, N. C.; Haight, H. L.; Doyle, J. R. Metal-Olefin Compounds. VII. The Crystal and Molecular Structure of Cyclo-tetra-$\mu$-chloro-tetrakis[bicyclo[2.2.1.]hepta-2$\pi$,5- dienecopper(I)]. *Inorg. Chem.* **1964**, *3* (11), 1535−1541.
(51) Kok, J. M.; Lim, K. C.; Skelton, B. W.; White, A. H. Lewis-Base Adducts of Group 11 Metal(I) Compounds. LXXVI Structural Studies in the Copper(I) Halide : Norbornadiene System. *J. Cluster Sci.* **2004**, *15* (3), 377−386.
(52) Lorber, C. Y.; Youinou, M.-T.; Kress, J.; Osborn, J. A. Isomerization of 2-methyl-3-butyn-2-ol into prenal: mechanistic observations on tricomponent catalyst systems of the type $Ti(OR)_4{-}CuCl{-}R'CO_2H$. Crystal Structure of $[CuCl(Me_2C(OH)CCH)]_4$. *Polyhedron* **2000**, *19* (14), 1693−1698.
(53) Mak, T. C. W.; Wong, H. N. C.; Hung Sze, K.; Book, L. Metal $\pi$-Complexes of Cyclooctatetraenes: V. Synthesis and X-Ray Analysis of Tetrameric Dibenzo[*a*,*e*]Cyclooctatetraenecopper(1) Chloride, a New "Step" Configuration for the $Cu_4Cl_4$ Ring. *J. Organomet. Chem.* **1983**, *255* (1), 123−134.
(54) Nardin, G.; Randaccio, L. The Crystal and Molecular Structure of the Dichloroethane Solvate of the 2:1 Derivative of Copper(I) Chloride and Bis(diphenylphosphino)methane. *Acta Crystallogr., Sect. B: Struct. Crystallogr. Cryst. Chem.* **1974**, *30* (5), 1377−1379.
(55) Ahuja, R.; Nethaji, M.; Samuelson, A. G. Chelating and Bridging Diphosphinoamine $(PPh_2)_2N(IPr)$ Complexes of Copper(I). *J. Organomet. Chem.* **2009**, *694* (7), 1144−1152.
(56) Dużak, T.; Zarychta, B.; Olijnyk, V. V. Coordination Environment Friendly Silicon in Copper(I) Chloride $\pi$-Complexes with Tetravinylsilane and Dimethyltetravinyldisiloxane. *Inorg. Chim. Acta* **2011**, *365* (1), 235−239.
(57) Schmidt, G.; Schittenhelm, N.; Behrens, U. Metallorganische Verbindungen des Kupfers VIII. Untersuchungen über die Koordinationschemie von heteroatomverbrückten Bisalkinen am Beispiel von Kupfer(I)-Halogenid- und -Trifluormethylsulfonat-Komplexen. *J. Organomet. Chem.* **1995**, *496* (1), 49−58.
(58) Cui, Y.; Chen, J.; Chen, G.; Ren, J.; Yu, W.; Qian, Y. Bis(2,2-bipyridine-N,N′)tetra-$\mu$-chloro-tetracopper(I). *Acta Crystallogr., Sect. C: Cryst. Struct. Commun.* **2001**, *57* (4), 349−351.
(59) Chen, Y.; Li, L.; Cao, Y.; Wu, J.; Gao, Q.; Li, Y.; Hu, H.; Liu, W.; Liu, Y.; Kang, Z.; Li, J. $Cu^{II}$-Mediated Controllable Creation of Tertiary and Quaternary Carbon Centers: Designed Assembly and Structures of a New Class of Copper Complexes Supported by *in situ* Generated Substituted 1-Pyridineimidazo[1,5-*a*]Pyridine Ligands. *CrystEngComm* **2013**, *15* (14), 2675−2681.
(60) Moreno, Y.; Spodine, E.; Vega, A.; Saillard, J.-Y. Structure and Bonding in the Hydrothermally Synthesized Copper(I) Complex $Cu_4(_2\text{-}Cl)_4(BIPY)_2$. *Inorg. Chim. Acta* **2003**, *350*, 651−655.
(61) Liu, H.-Y.; Yu, Z.-T.; Yuan, Y.-J.; Yu, T.; Zou, Z.-G. Efficient N-Arylation Catalyzed by a Copper(I) Pyrazolyl-Nicotinic Acid System. *Tetrahedron* **2010**, *66* (47), 9141−9144.
(62) Collins, L. R.; Lowe, J. P.; Mahon, M. F.; Poulten, R. C.; Whittlesey, M. K. Copper Diamidocarbene Complexes: Characterization of Monomeric to Tetrameric Species. *Inorg. Chem.* **2014**, *53* (5), 2699−2707.
(63) Yang, X.-Y.; Li, Y.; Pullarkat, S. A. A One-Pot Diastereoselective Self Assembly of C-Stereogenic Copper(I) Diphosphine Clusters. *Inorg. Chem.* **2014**, *53* (19), 10232−10239.
(64) Leschke, M.; Lang, H.; Holze, R. Electronic Interactions in Copper(I) and Silver(I) Complexes between the Ligands and Metals as Evidenced with Cyclic Voltammetry. *Electrochim. Acta* **2003**, *48* (7), 919−924.


https://doi.org/10.1021/acs.organomet.1c00231
*Organometallics* 2021, 40, 2090−2099